

**PERCENTAGE DEPTH DOSE (PDD) OF 9 MEV
ELECTRON BEAM IN THE MEDIUM WITH THE
PRESENCE OF INHOMOGENEOUS TISSUE BY
USING OPTICALLY STIMULATED
LUMINESCENCE DOSIMETER (OSLD), EBT3
FILM AND IONIZATION CHAMBER**

NUR SYAZWANY BINTI MALEK

**SCHOOL OF HEALTH SCIENCES
UNIVERSITI SAINS MALAYSIA**

2024

**PERCENTAGE DEPTH DOSE (PDD) OF 9 MEV
ELECTRON BEAM IN THE MEDIUM WITH THE
PRESENCE OF INHOMOGENEOUS TISSUE BY
USING OPTICALLY STIMULATED
LUMINESCENCE DOSIMETER (OSLD), EBT3
FILM AND IONIZATION CHAMBER**

By

NUR SYAZWANY BINTI MALEK

**Dissertation submitted in fulfilment of the requirement for the degree of
Bachelor of Health Sciences (Honours) (Medical Radiation)**

July 2024

CERTIFICATE

This is to certify that the dissertation entitled “**PERCENTAGE DEPTH DOSE (PDD) OF 9 MEV ELECTRON BEAM IN THE MEDIUM WITH THE PRESENCE OF INHOMOGENEOUS TISSUE BY USING OPTICALLY STIMULATED LUMINESCENCE DOSIMETER (OSLD), EBT3 FILM AND IONIZATION CHAMBER**” is the bona fide record of research work done by NUR SYAZWANY BINTI MALEK during the period from October 2023 to July 2024 under my supervision. I have read this dissertation, and I agree that in my opinion, it conforms to acceptable standards of scholarly presentation and is fully adequate in scope and quality as a dissertation to be submitted in partial fulfillment for the degree of Bachelor of Health Science (Honours) (Medical Radiation).

Main supervisor,

.....

Dr. Mohd Fahmi Bin Mohd Yusof

Senior Lecturer,

School of Health Sciences,

Universiti Sains Malaysia,

16150 Kubang Kerian,

Kelantan,

Date: 8 August 2024

Co-Supervisor,

.....

Cik Arifah Nazirah Binti Abdullah

Medical Physicist,

School of Health Sciences,

Universiti Sains Malaysia,

16150 Kubang Kerian,

Kelantan.

Date: 8 August 2024

Field Supervisor,

.....

En. Ahmad Bazlie Bin Abdul Kadir

Research Officer,

Secondary Standard Dosimetry

Laboratory (SSDL),

Radiation Metrology Group,

Radiation Safety and Health Division,

Malaysian Nuclear Agency,

4300 Bangi Kajang,

Selangor.

Date: 8 August 2024

Field Supervisor,

.....

Pn. Norriza Binti Mohd Isa

Research Officer,

Medical Physics Laboratory (MPL),

Radiation Metrology Group,

Radiation Safety and Health Division,

Malaysian Nuclear Agency,

4300 Bangi Kajang,

Selangor.

Date: 8 August 2024

DECLARATION

I hereby declare that this dissertation is the result of my investigation, except where otherwise stated and duly acknowledged. I also declare that it has not been previously or concurrently submitted as a whole for any other degrees at Universiti Sains Malaysia (USM) or other institutions. I acknowledged that the research work and collection of data belong to the Universiti Sains Malaysia.

.....

NUR SYAZWANY BINTI MALEK

Date: 8 August 2024

ACKNOWLEDGMENT

I want to extend my deepest gratitude to Allah SWT for providing me with the opportunity and continuous support in completing my research on the Percentage Depth Dose (PDD) of 9 MeV Electron Beam in The Medium with The Presence of Inhomogeneous Tissue by Using Optically Stimulated Luminescence Dosimeter (OSLD), EBT3 Film and Ionization Chamber

I am deeply grateful to my main supervisor, Dr. Mohd Fahmi Bin Yusof, for his invaluable guidance and assistance throughout this research project. I also thankful to my co-supervisor, Cik Arifah Nazirah Binti Abdullah, for her significant role in supervising and guiding me using the linear accelerator for data collection at Hospital Universiti Sains Malaysia (HUSM). Additionally, I wish to acknowledge my field supervisors from the Malaysian Nuclear Agency (Nuclear Malaysia), En. Ahmad Bazlie Bin Abdul Kadir and Pn. Norriza Binti Mohd Isa from Nuclear Malaysia, for their guidance regarding the dosimetry of OSLD. I am also thankful to the Department of Nuclear Medicine, Radiotherapy, and Oncology at HUSM for granting me access to their equipment during my research.

I want to thank my parents and friends for their moral support and helps during data collection and the dissertation drafting process. Lastly, I want to acknowledge myself for the perseverance and dedication I exhibited throughout this journey. I thank myself for believing in myself, for my relentless effort, and for never giving up.

TABLE OF CONTENTS

CERTIFICATE	iii
DECLARATION	iv
ACKNOWLEDGMENT	v
TABLE OF CONTENTS	vi
LIST OF TABLES	x
LIST OF FIGURES	xii
LIST OF SYMBOLS.....	xvi
LIST OF ABBREVIATIONS	xvii
LIST OF APPENDICES.....	xviii
ABSTRAK	xix
ABSTRACT	xx
CHAPTER 1 INTRODUCTION.....	1
1.1 Background of Study.....	1
1.2 Problem Statement	4
1.3 Objectives.....	5
1.4 Hypothesis.....	5
1.5 Significant of Study.....	6
CHAPTER 2 LITERATURE REVIEW	7
2.1 Megavoltage Electron Beam	7
2.2 Percentage Depth Dose (PDD).....	9
2.3 Optically Stimulated Luminescence Dosimeter (OSLD).....	14
2.4 Radiochromic Film.....	16

2.5	Ionization Chamber	18
2.6	Previous Studies	20
CHAPTER 3 MATERIAL AND METHODOLOGY.....		25
3.1	Materials.....	25
3.1.1	Varian Ix Linear Accelerator	25
3.1.2	Solid Water Phantom.....	25
3.1.3	Bone Equivalent Phantom.....	26
3.1.4	Cork (Lung) Equivalent Phantom	27
3.1.5	Superflab Bolus.....	27
3.1.6	OSLD	28
3.1.7	MicroStar Reader	29
3.1.8	Manual Optical Annealer	30
3.1.9	Ionization Chamber.....	30
3.1.10	Gafchromic EBT3 Film	31
3.1.11	Epson Expression 1000 XL Film Scanner	32
3.2	Methodology	33
3.2.1	Preparation of OSLD	34
3.2.1(a)	Calibration of OSLD and MicroStar Reader.	35
3.2.1(b)	Annealing of OSLD.....	36
3.2.1(c)	Initial Reading of OSLD.....	37
3.2.2	Calibration of EBT3 Film	40
3.2.2(a)	Preparation of EBT3 Film	41
3.2.2(b)	Irradiation of EBT3 Film.....	42
3.2.2(c)	Scanning of EBT3 Film.....	44
3.2.3	Dose Linearity of OSLD	46
3.2.4	Preparation of Phantom for PDD Measurement	48

3.2.4(a)	Solid Water Phantom Setup	48
3.2.4(b)	Solid Water-Bone Phantom Setup	49
3.2.4(c)	Solid Water-Cork (Lung) Phantom Setup.....	50
3.2.5	Measurement of the PDD by Using OSLD, EBT3 Film and Ionization Chamber	51
3.2.5(a)	PDD in Solid Water Phantom by Using OSLD, EBT3 Film and Ionization Chamber	51
3.2.5(b)	PDD in Solid Water-Bone Phantom Setup and Solid Water-Cork (Lung) Phantom Setup by Using OSLD and EBT3 Film.	55
3.2.6	Post-Irradiation Absorbed Dose Analysis	57
3.2.6(a)	Ionization Chamber Dose Analysis	57
3.2.6(b)	OSLD Dose Analysis.....	58
3.2.6(c)	EBT3 Film Dose Analysis	58
3.2.7	Calculation and Comparison of PDD Measurement By OSLD, EBT3 Film, And Ionization Chamber	59
3.2.8	Statistical Test of PDD Measurement by OSLD, EBT3 Film, and Ionization Chamber Using SPSS	60
CHAPTER 4	RESULT AND DISCUSSION.....	62
4.1	Calibration of EBT3 Film	62
4.2	Dose Linearity of Nanodot OSLD	63
4.3	PDD in Solid Water Phantom Setup	64
4.4	PDD in Solid Water-Bone Phantom Setup.....	66
4.5	PDD in Solid Water-Cork (Lung) Phantom Setup	69
4.6	Uncertainty With PDD Measurement Using EBT3 Film.....	71
4.7	Statistical Analysis of PDD Measurement by OSLD, EBT3 Film and Ionization Chamber	72

CHAPTER 5 CONCLUSION AND RECOMMENDATION FOR FUTURE WORK.....	74
5.1 Conclusion.....	74
5.2 Recommendations For Future Work	75
REFERENCES.....	76
APPENDICES.....	83

LIST OF TABLES

Table 2.1: Summary of the previous study with comparison to the present study.....	23
Table 4.1: Electron beam parameter for PDD in solid water phantom measured by using OSLD, EBT3 film, and ionization chamber.....	65
Table 4.2: Electron range parameter for PDD measured in solid water-bone setup by OSLD in comparison to EBT3 film.	68
Table 4.3: Electron range parameter for PDD measured in solid water-cork (lung) setup by OSLD in comparison to EBT3 film.....	71
Table 4.4: The Mann-Whitney test between the PDD in OSLD and the ionization chamber measured in a solid water phantom setup.....	73
Table 4.5: The Mann-Whitney test between the PDD in OSLD and EBT3 film measured in a solid water phantom, solid water-bone phantom, and solid water-cork phantom setup.	73
Table 5.1: The list of EBT3 film used for EBT3 film calibration.....	83
Table 5.2: The pixel value obtained at increasing dose (cGy) for EBT3 film calibration	83
Table 5.3: The list of OSLD used for the dose linearity test of OSLD.....	84
Table 5.4: The dose obtained by OSLD at increasing MU for dose linearity of OSLD	84
Table 5.5: The list of OSLD and EBT3 films used for PDD measurement in solid water phantom.....	85
Table 5.6: Depth dose measurement in the solid water phantom setup by using an ionization chamber.....	86
Table 5.7: Depth dose measurement in the solid water phantom setup by using OSLD	86
Table 5.8: Depth dose measurement in the solid water phantom setup by using EBT3 film	86

Table 5.9: The list of OSLD and EBT3 films used for PDD measurement in solid water-bone phantom setup	87
Table 5.10: Depth dose measurement in the solid water-bone phantom setup by using OSLD	88
Table 5.11: Depth dose measurement in the solid water-bone phantom setup by using EBT3 film.....	88
Table 5.12: The list of OSLD and EBT3 films used for PDD measurement in solid water-cork (lung) phantom setup	89
Table 5.13: Depth dose measurement in the solid water-cork (lung) phantom setup by using OSLD	90
Table 5.14: Depth dose measurement in the solid water-cork (lung) phantom setup by using EBT3 film.....	90

LIST OF FIGURES

Figure 2.1: Schematic diagram illustrates the beam production by linear accelerator (Kotha et al., 2021)	7
Figure 2.2: Schematic diagram illustrates the PDD measurement in water phantom (Sruti et al., 2015)	10
Figure 2.3: Comparison of PDD curve shape in water phantom between (a) electron and (b) photon (Mayles, Nahum & Rosenwald, 2021)	11
Figure 2.4: Typical electron range parameter used in defining electron PDD curve.	12
Figure 2.5: Electron PDD curve in inhomogeneous density medium containing bone material (Xiaofang Wang, 1994)	13
Figure 2.6: Electron PDD curve in inhomogeneous density medium containing lung material (Mihailescu, Borcia & Alexandru, 2018)	13
Figure 2.7: Schematic diagram illustrates the fundamental principle of OSLD during (a) reading and (b) irradiation (Takegami et al., 2015)	15
Figure 2.8: Schematic diagram illustrates the composition of EBT3 film (Rohani et al., 2019)	17
Figure 2.9: Example of film darkening as the dose increases (Musa et al., 2022)	17
Figure 2.10: Schematic diagram illustrates the component of parallel plate ionization chamber (Maia & Caldas, 2005)	19
Figure 2.11: Schematic diagram illustrates the fundamental principle of the ionization chamber	20
Figure 3.1: Linear accelerator used to produce 9 MeV electron beam for irradiation.	25
Figure 3.2: Solid water phantom used to simulate the human soft tissue density.....	26
Figure 3.3: Bone equivalent phantom used to simulate human compact bone density.	27
Figure 3.4: Cork (lung) equivalent phantom used to simulate human lung density. .	27

Figure 3.5: Superflab bolus used to eliminate air gaps between phantoms.	28
Figure 3.6: NanoDot OSLD used to measure PDD	29
Figure 3.7: MicroStar reader used to read the OSLD	29
Figure 3.8: Optical manual annealer used to reset the signals in OSLD.	30
Figure 3.9: Advanced Markus ionization chamber inside Markus base plate to measure PDD	31
Figure 3.10: Electrometer used to obtain ionization charge reading	31
Figure 3.11: Example of EBT3 film cut into small pieces to measure PDD	32
Figure 3.12: Epson expression 1000xl film scanner used to scan irradiated film	33
Figure 3.13: Flowchart demonstrates the steps for PDD measurement.....	33
Figure 3.14: Flowchart demonstrates the process for data collection.....	34
Figure 3.15: Flowchart demonstrates the preparation of OSLD before data acquisition.	35
Figure 3.16: Reader calibration factor for low and high doses of therapeutic energy range.....	36
Figure 3.17: The placement of the nanoDot OSLD in the manual annealer for the annealing process	37
Figure 3.18: MicroStar reader setting at the configuration tab (a) dosimeter type choose nanoDot (b) reading unit choose SI unit.....	38
Figure 3.19: The placement of nanoDot OSLD inside (a) holder and (b) loader	39
Figure 3.20: MicroStar reader setting at the (a) reading tab to insert the serial number and (b) export tab to export the data.....	40
Figure 3.21: Flowchart demonstrates the process for EBT3 film calibration.....	41
Figure 3.22: Schematic diagram illustrates the preparation of EBT3 film for data acquisition	42
Figure 3.23: Schematic diagram illustrates the experimental setup for EBT3 film...	42
Figure 3.24: The position of EBT3 film at the beam central axis during film calibration.	43

Figure 3.25: The position of EBT3 film on the scanner platform for post-irradiation scanning procedure.	44
Figure 3.26: “FilmScan” software interface showed (a) a preview of the film before scanning and (b) scanning parameters	45
Figure 3.27: “FilmCal” software interface showed (a) ROI function and (b) table of dose to pixel value	46
Figure 3.28: Schematic diagram illustrates the experimental setup for dose linearity of OSLD	47
Figure 3.29: The position of OSLD at the beam central axis during the dose linearity of OSLD	48
Figure 3.30: Solid water phantom setup (a) schematic diagram (b) actual phantom.	49
Figure 3.31: Solid water-bone phantom setup (a) schematic diagram (b) actual phantom.....	50
Figure 3.32:: Solid water-cork (lung) phantom setup (a) schematic diagram (b) actual phantom.	50
Figure 3.33: Flowchart demonstrates the PDD measurement in solid water phantom by using three different dosimeters.....	51
Figure 3.34: Experimental setup for PDD measurement in solid water phantom setup (a) schematic diagram (b) actual setup.....	52
Figure 3.35: The placement of dosimeter at beam central axis during PDD measurement (a) Markus ion chamber (b) nanoDot OSLD and (c) EBT3 film.	54
Figure 3.36: The placement of bolus on top of the dosimeter during PDD measurement.	55
Figure 3.37: Experimental setup for PDD measurement in solid water-bone phantom setup (a) schematic diagram (b) actual setup.....	56
Figure 3.38: Experimental setup for PDD measurement in solid water-cork (lung) phantom setup (a) schematic diagram (b) actual setup.....	56

Figure 3.39: Table of depth to absorbed dose for each film.....	59
Figure 3.40: Example of extrapolated PDD curve to estimate the electron parameter	60
Figure 3.41: Example of data input at data view by using SPSS.....	61
Figure 4.1: EBT3 film calibration curve (pixel value vs dose) for 9 MeV electron beam	62
Figure 4.2: Graph illustrates the dose linearity of OSLD	63
Figure 4.3: PDD curve in solid water phantom measured by using OSLD, EBT3 film, and ionization chamber	64
Figure 4.4: PDD curve in solid water-bone phantom measured by using OSLD and EBT3 film	67
Figure 4.5: PDD curve in solid water-cork (lung) phantom setup measured by using an OSLD and EBT3 film	69

LIST OF SYMBOLS

$\text{Al}_2\text{O}_3\text{:C}$	Aluminium Oxide Doped with Carbon
cm	Centimeter
cGy	Centigray
$^{\circ}\text{C}$	Celsius
^{60}Co	Cobalt-60
^{137}Cs	Caesium-137
d_{max}	Maximum Dose
keV	Kilovoltage
MeV	Megavoltage
mGy	Milligray
nC	Nano Coulomb
nm	Nanometer
R^2	Linear Regression Value
R_{80}	Depth of 80 % Dose Level
R_{50}	Depth of 50 % Dose Level
R_P	Practical Range
R_t	Therapeutic Range
Z	Atomic Number
V	Voltage
Z_{max}	Depth Of Maximum Dose
μm	Micrometer

LIST OF ABBREVIATIONS

AXB	Acuros XB
CF	Calibration Coefficient
CM	Centimeter
EBT	External Beam Radiotherapy
HUSM	Hospital Universiti Sains Malaysia
LED	Light-Emitting Diodes
LET	Linear Energy Transfer
MU	Monitor Unit
MC	Monte Carlo
MPL	Medical Physics Laboratory
Nuclear Malaysia	Malaysian Nuclear Agency
OD	Optical Density
OSLD	Optically Stimulated Luminescence Dosimeter
PC	Personal Computer
PDD	Percentage Depth Dose
PMT	Photomultiplier Tube
PPSK	Pusat Pengajian Sains Kesihatan
SSDL	Secondary Standard Dosimetry Laboratory
SSD	Source to Surface Distance
SPSS	Statistical Package for the Social Science
TPS	Treatment Planning System
TLD	Thermoluminescent Dosimeter
USM	Universiti Sains Malaysia

LIST OF APPENDICES

- Appendix A Measurement for EBT3 Film Calibration
- Appendix B Measurement for Dose Linearity of OSLD
- Appendix C Measurement of PDD in Solid Water Phantom Setup Measured
by An Ionization Chamber, OSLD, and EBT3 Film
- Appendix D Measurement of PDD in Solid Water-Bone Phantom Setup
Measured by OSLD and EBT3 Film
- Appendix E Measurement of PDD in Solid Water-Cork (Lung) Phantom Setup
Measured by OSLD, and EBT3 Film

**PERATUSAN DOSE KEDALAMAN (PDD) UNTUK SINAR ELECTRON
9 MEV DALAM MEDIUM YANG MEMPUNYAI KEPADATAN TISU TIDAK
SERAGAM MENGGUNAKAN DOSIMETER LUMINESENS STIMULASI
OPTIK (OSLD), FILEM EBT3 DAN KEBUK PENGIONAN**

ABSTRAK

Tubuh manusia mempunyai variasi dalam kepadatan tisu seperti tisu tulang yang berkepadatan tinggi dan tisu paru-paru yang berkepadatan rendah, akan mempengaruhi taburan dos di dalam medium. Kajian ini dijalankan untuk menilai ketepatan dosimetri dosimeter luminesens stimulasi optik (OSLD) untuk mengesan dan mengukur gangguan dos di dalam medium. Kajian ini dijalankan untuk mengukur peratusan dos kedalaman (PDD) dalam tiga tetapan medium yang terdiri daripada medium air, tulang dan gabus (paru paru) . Tiga tetapan medium iaitu tetapan air sahaja, tetapan air-tulang dan tetapan air-gabus (paru-paru) telah didedahkan kepada sinaran elektron 9 MeV dan PDD diukur dengan menggunakan OSLD, filem EBT3 dan kebuk pengionan. Lengkung PDD serta parameter julat electron dibandingkan antara dosimeter dan ujian statistik telah dibuat untuk mendapatkan nilai *p* bagi menilai persetujuan antara PDD. Hasil kajian menunjukkan bahawa PDD yang diukur oleh OSLD mengampiri PDD yang diukur oleh kebuk pengionan dan filem EBT3 dalam tetapan air sahaja. PDD dalam tetapan air-tulang dan air-gabus yang dikur oleh OSLD mempamerkan bentuk yang konsisten dengan EBT3 film dan selari dengan kajian terdahulu. Tiada perbezaan yang ketara diperhatikan antara PDD OSLD dengan filem EBT3 dan kebuk pengionan, dibuktikan dengan nilai-*p* > 0.05 yang diperoleh dari ujian statistik. Kesimpulannya, OSLD sesuai digunakan sebagai dosimeter pasif untuk dosimetri elektron bertenaga tinggi dalam medium yang mempunyai ketumpatan tisu tidak seragam.

**PERCENTAGE DEPTH DOSE (PDD) OF 9 MEV ELECTRON BEAM IN
THE MEDIUM WITH THE PRESENCE OF INHOMOGENEOUS TISSUE BY
USING OPTICALLY STIMULATED LUMINESCENCE DOSIMETER
(OSLD), EBT3 FILM AND IONIZATION CHAMBER**

ABSTRACT

The human body has variations in tissue density such as high-density bone tissue and low-density lung tissue, which will impact the dose distribution in the medium. The study aims to evaluate the dosimetric accuracy of optically stimulated luminescence dosimeters (OSLD) and their ability to detect and measure dose perturbation by measuring the percentage depth dose (PDD) in the medium consisting of solid water, bone equivalent, and cork(lung) equivalent phantom. Three phantom setups of solid water phantom, solid water-bone phantom, and solid water-cork (lung) phantom were irradiated with a 9 MeV electron beam, and the PDD was measured using OSLD, EBT3 film, and ionization chamber. The PDD curve and electron range parameter obtained by OSLD was compared to other dosimeters and statistical test was conducted to determine the agreement between the PDD using the p -value. The results showed that PDD measured by OSLD was in good agreement with the ionization chamber and EBT3 film dosimetry in a homogenous solid water phantom setup. PDD in the inhomogeneous solid water-bone and solid water cork (lung) phantom setups measured by OSLD was also consistent with the EBT3 film and previous studies. No significant differences were observed between PDD measured by OSLD and the reference dosimetry, evidenced by p -value > 0.05 obtained from statistical tests. The overall results indicated the suitability of OSLD as a passive dosimeter in electron beam dosimetry in the medium with the presence of inhomogeneous tissue.

CHAPTER 1

INTRODUCTION

1.1 Background of Study

In external beam radiotherapy, a linear accelerator will produce high-energy photon or electron beams precisely aimed at a specific distance from the patient to eradicate cancer cells and hinder their capacity to proliferate and divide (Koka *et al.*, 2022). High-energy photon beams are commonly employed in treating deep-seated tumors due to their benefits, including a skin-sparing effect and increased tissue penetration capabilities (Breitkreutz, Weil & Bazalova-Carter, 2020). Electron beams offer advantages over photon beams due to their higher linear energy transfer (LET) and reduced penetration power, making them suitable for treating superficial or semi-deep-seated tumors near the skin's surface, such as radiation boost to the breast tumor bed (Jong *et al.*, 2018). The combination of high surface dose, coupled with a rapid dose reduction beyond the 80% dose range leads to an overall improvement in the likelihood of tumor control and a decrease in normal tissue complications for superficial tumors (Mutsakanyi & du Plessis, 2021). The effectiveness of the treatment depends on the accuracy of the treatment planning process, but the precision of dose calculation tends to be compromised when dealing with an inhomogeneous density medium (Parenica *et al.*, 2019).

The human body exhibits inhomogeneity due to its composition of diverse tissues and cavities, each having distinct densities, atomic numbers, scattering, and absorption properties (Verma *et al.*, 2019). A prime example is the chest area, which comprises high-density bones, soft tissue, low-density lung tissue, and air cavities. These variations can impact the distribution of doses within the irradiated volume and

must be considered during the development of the treatment plan. The distribution of dose at interfaces between materials of varying densities can be affected due to the backscattering process, which can cause either an increase or decrease in dose (Azizi *et al.*, 2019). High-density tissue such as bone attenuates electron beams, leading to a reduction in dose beyond the bone and an increased dose in front of the bone (Parwaie *et al.*, 2022). In contrast, there is less energy absorption by low-density tissue such as the lung thus increasing the absorbed dose beyond it (Zabihzadeh *et al.*, 2020). Since dose calculations can be imprecise when tissue inhomogeneity is disregarded, measuring dose perturbation within, beyond, in front of, and laterally around the inhomogeneity is crucial to ensure accurate dose delivery and effective treatment.

Dose perturbation can be determined by measuring the medium's percentage depth dose (PDD). This is because the information about absorbed dose distribution within a patient is commonly characterized by PDD and beam dose profiles or off-axis ratios (Bencheikh, Maghnouj & Tajmouati, 2020). PDD is a critical parameter that helps evaluate a medium's attenuation properties and a dosimeter's detection characteristics. In the presence of inhomogeneities, the shape of the PDD curve can experience significant changes. Aside from treatment planning system (TPS) calculations and Monte Carlo (MC) simulations, PDD can also be indirectly determined through measurements in phantom by using a dosimeter. PDD is often measured in a homogeneous medium such as a water phantom using an ionization chamber and a radiochromic film (Robinson *et al.*, 2020). However, according to previous studies, PDD measurements in the inhomogeneous medium have been measured using a thermoluminescence dosimeter (TLD), ionization chamber, and radiochromic films.

With advancements in technology, a small type of commercial aluminium oxide doped with carbon ($\text{Al}_2\text{O}_3:\text{C}$) optically stimulated luminescence (OSL) nanoDot dosimeters was produced by Landauer, Inc. in Glenwood, IL, and it has been proven as effective dosimeters for in vivo dosimetry (Raj *et al.*, 2021). OSLD offers several advantages compared to other dosimeters such as it offers high spatial resolution due to its small size and it allows for multiple readings with minimal signal loss (Hoshida *et al.*, 2019). Additionally, OSLD covers a wide energy range from 5 keV to 20 MeV and exhibits good linearity as dose levels increase (Kara & Hicsonmez, 2022). The OSLD demonstrates high accuracy and precision in dose determination, and it maintains reusability and readability even after extended periods of irradiation. However, a drawback is that the phosphor material is sensitive to light, but it is effectively addressed by using a water-equivalent light-tight plastic encapsulation (Ponmalar *et al.*, 2017).

Limited research has been conducted on the application of the OSLD for PDD measurement in the inhomogeneous density medium under high-energy electron beams. Therefore, this study conducts a PDD measurement in three phantom setups. Two setups for inhomogeneous density mediums consisting of either bone or cork (lung) equivalent phantom sandwiched between solid water phantom measured by using OSLD and EBT3 film while one setup for homogenous density medium consisting of only solid water phantom measured by using OSLD, EBT3 film, and an ionization chamber. The PDD obtained by OSLD for each setup is compared to other dosimeters and PDD obtained in the homogenous density medium is compared to PDD in the inhomogeneous density medium to determine the difference in dose distribution. Overall, this study aims to determine the suitability of the OSLD for dosimetry in medium with the presence of inhomogeneous tissue under high-energy electron beams in comparison to other dosimeter.

1.2 Problem Statement

Variations in tissue density such as high-density bone tissue and low-density lung tissue lead to different levels of attenuation of ionizing radiation which can affect the dose distribution along the pathway of electron beams, resulting in undesired fluctuations in radiation transmission, particularly at interfaces and beyond the inhomogeneity. This will cause inaccurate dose delivery to the target volume and surrounding healthy tissue. The impact of inhomogeneity can be observed through PDD measurement since the inhomogeneity will influence and modify the shape of the PDD curve.

There is no practical method to directly measure dose distribution within the human body due to the impracticality of placing a dosimeter inside the body. However, an indirect approach involves computer-based simulations such as TPS and MC simulation techniques to calculate dose distribution in the medium. Despite significant advancements in computer-based methods, they primarily rely on simulations and predictions, which may introduce biases and errors. Furthermore, while MC simulation is regarded as the gold standard suggested by previous studies for dose calculation involving inhomogeneities, its time-consuming nature renders it impractical for clinical use.

Given the constraints of TPS and MC simulation, an alternative indirect approach involves conducting dose measurements in an inhomogeneous density phantom using a dosimeter. Limited information is available regarding the application of passive dosimeters to measure the effect of inhomogeneity on dose distribution. Past studies have employed passive dosimeters like TLD and film. Although OSLD have been proven as effective dosimeter for electron beam dosimetry due to its advantages

such as small size and it allows for multiple readings with minimal signal loss but there is limited research on the utilization of OSLD for measuring PDD in medium with presence of inhomogeneous tissue under high-energy electron beams. Therefore, this study aims to investigate whether OSLD can effectively detect and measure dose perturbation in medium with the presence of an inhomogeneous tissue under a high-energy electron beam.

1.3 Objectives

The general objective of this study is to measure PDD of 9 MeV electron beam in the medium with the presence of bone equivalent phantom and cork (lung) equivalent phantom by using OSLD and EBT3 film. This study also measures PDD in the homogenous solid water phantom by using OSLD, EBT3 film and ionization chamber.

The specific objectives of this study are:

- 1) To plot and compare the PDD curve obtained by OSLD in comparison to EBT3 film and ionization chamber in each phantom setup.
- 2) To determine and compare the electron range parameter extrapolated from the PDD curve between OSLD, EBT3 film and ionization chamber in each phantom setup.
- 3) To calculate the p -value and evaluate the agreement of PDD value measured by OSLD in comparison to EBT3 film and ionization chamber in each phantom setup by using statistical test.

1.4 Hypothesis

The null hypothesis of this study is there is no significant difference in PDD measured by OSLD in comparison to EBT3 film and ionization chamber in the medium with the presence of inhomogeneous tissue.

The alternative hypothesis of this study is there is a significant difference in PDD measured by OSLD in comparison to EBT3 film and ionization chamber in the medium with the presence of inhomogeneous tissue.

1.5 Significant of Study

The adoption of OSLD for in vivo dosimetry is rapidly growing, showing significant promise as a passive dosimeter, especially in radiotherapy applications. However, there is a lack of research examining its effectiveness in addressing dose perturbation caused by tissue inhomogeneities. This study aims to fill this gap by investigating the use of OSLD as a passive dosimeter for PDD measurement in the inhomogeneous density mediums under high-energy electron beams. The study aims to validate the accuracy of OSLD for measuring dose perturbation by comparing the results with those obtained from EBT3 film and ionization chambers. This comparative analysis will strengthen the study's findings and enhance confidence in the reliability of OSLD for this specific application. This study not only addresses this knowledge gap but also contributes to understanding the differences in dose distribution within mediums of varying densities.

CHAPTER 2

LITERATURE REVIEW

2.1 Megavoltage Electron Beam

Since the 1950s, radiotherapy has employed high-energy electrons due to their high LET which induces greater chemical changes in DNA compared to photons. This capability can result in damage to superficial cancerous cells. The electron energy ranges from 6 to 20 MeV have widely been used due to their precise control over radiation penetration depth and reduced impact on deeper tissues. (Apipunyasopon *et al.*, 2020). Presently, modern linear accelerators can generate multiple electron beam energies alongside two or more photon energies. The electron beam undergoes several processes inside the gantry before entering the treatment head where clinical beams are produced as shown in **Figure 2.1**.

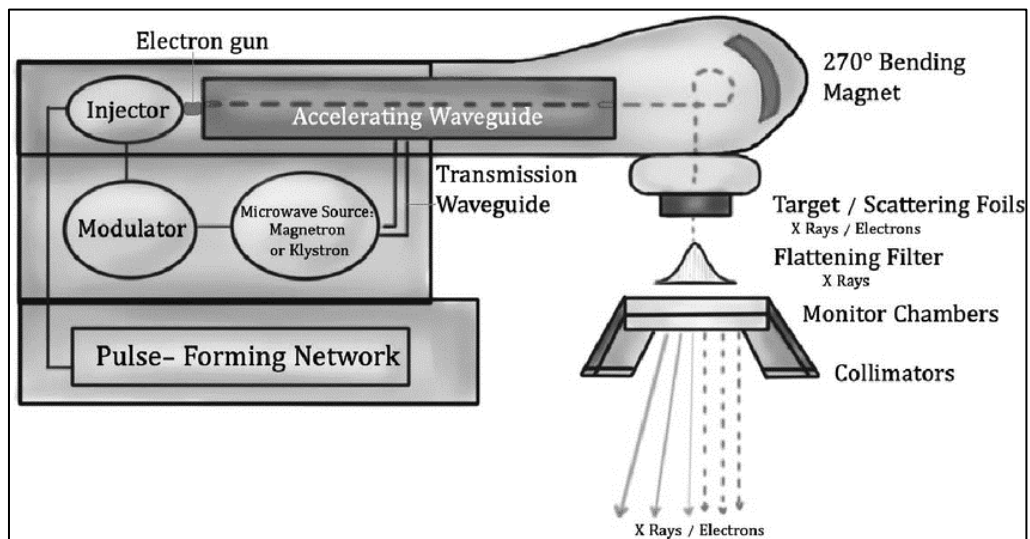


Figure 2.1: Schematic diagram illustrates the beam production by linear accelerator

(Kotha et al., 2021)

Electron gun generates electron and accelerate them in the accelerating waveguide until they achieve the desired kinetic energy. They will travel as a pencil

beam through the beam transport system into the treatment head via a thin window made of from low atomic number (Z) material which minimizes scattering and the production of bremsstrahlung radiation. In the treatment head, scattering foils will replace the target and the flattening filter to activate the electron beam mode. Once the electrons pass through the scattering foil, they will scatter significantly due to the interaction with the machine component, air, and the patient, thus leading to an undesirable penumbra in clinical settings (Mayles, Nahum & Rosenwald, 2021). Since the positioned of the photon beam collimators is too distant from the patient for efficient field shaping, therefore during the treatment uses electron applicators to stop large-angle scatter electrons and provide a uniform dose within 80% of the field width (Sengupta et al., 2024).

Electron beams exhibit unique physical characteristics that distinguish them from photon beams. For example, they carry a negative (-) charge which categorizing them as a directly ionizing radiation which deposit energy directly into the medium through Coulomb force interactions with atom. Besides, they have low mass of approximately 9.109×10^{-31} kilograms, which causes easy deflection of electrons from the original path. As electron beam travel through a medium, their energy gradually dissipates, eventually reaching thermal energies and scattering from its initial trajectory. Deposition of dose within the medium relies on the energy transfer from electrons. In the medium, electrons will interact with either orbital electrons or the nucleus of the atom in two main ways of either elastic or inelastic collision. (Mihailidis, 2019).

In inelastic collision, kinetic energy is lost through ionization, excitation, or conversion to bremsstrahlung photons while in elastic collision, kinetic energy is not lost but may be redistributed among the particles involved. Electrons typically lose

approximately 2 MeV/cm of energy in a water medium. In low Z material, electrons lose energy mainly through inelastic collisions with atomic electrons, resulting in ionization or excitation events called collisional losses. However, in high Z materials, energy losses become more prominent due to bremsstrahlung production called radiative losses. During the inelastic collision with atomic electrons, the ejected is known as a delta ray if the electron gains sufficient energy to trigger additional ionizations at a distance from the initial interaction point (Mott & Daniel, 2021).

The electrons' energy level and the material's electron density influence the amount of energy lost from collisions. The mass stopping power, which is the rate of energy loss per gram per centimeter squared, is greater for materials with low Z values compared to materials with high Z values. It is because high Z materials have a lower electron density per gram and stronger binding, which reduces their availability for interactions. Furthermore, the energy loss rate for radiative interaction is dependent on both the electron energy and the absorbers' atomic number squared (Z^2). X-ray generation is more effective with electrons of greater energy and absorbent materials with higher atomic numbers (Mott & Daniel, 2021).

2.2 Percentage Depth Dose (PDD)

Percentage depth dose (PDD) is an important parameter used to analyze the dose distribution within a medium along the primary axis of a linear accelerator (Bilalodin & Abdullatif, 2022). PDD is an attenuation factor that characterizes the central axis dose distribution by normalizing the dose at a particular depth to the maximum dose. Based on **Figure 2.2**, PDD is defined as the ratio of the absorbed dose at any depth, Q to the absorbed dose at a fixed reference depth, P typically the maximum dose (d_{max}), along the beam's central axis (Sruti *et al.*, 2015). PDD measurement is usually conducted in

water phantom based on the source-to-surface distance (SSD) setup and the maximum PDD value is either 1 or 100%.

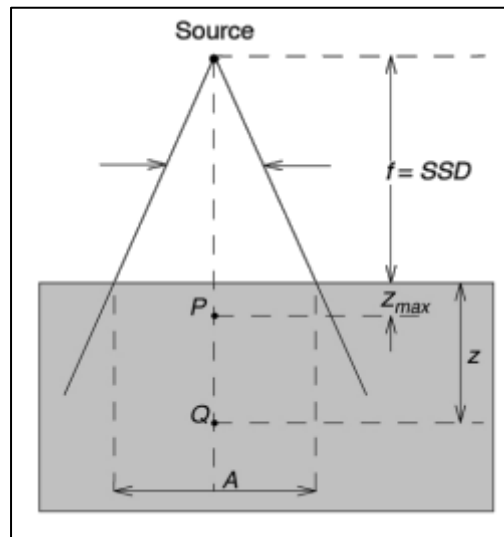


Figure 2.2: Schematic diagram illustrates the PDD measurement in water phantom
(Sruti *et al.*, 2015)

The PDD curve for electron beams exhibits a unique shape compared to photon beams as shown in **Figure 2.3**. This is primarily due to electrons and photons' different physical interactions with matter. The DD curve for electron beam features a high surface dose, rapid dose falls beyond the d_{max} , and the presence of bremsstrahlung tail caused by photon contamination. The shape of the PDD curve illustrates the dose distribution in the medium starting from the surface dose until the exit dose. Initially, as the beam penetrates the medium, it will deliver a high surface dose ranging from 80% to 90%, due to scattering interactions between the electrons and the atoms in the medium. As depth increases, the dose gradually rises, reaching a maximum dose at a specific depth and this region known as build up region. Then, the dose will decrease rapidly due to scattering and continuous energy loss and levels off at low-level dose components caused by photon contamination which is bremsstrahlung production (Mayles, Nahum & Rosenwald, 2021).

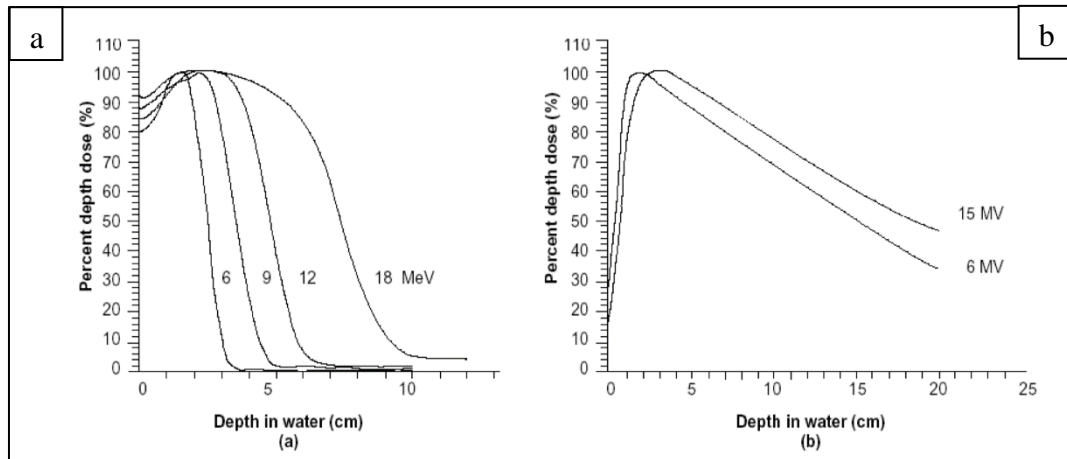


Figure 2.3: Comparison of PDD curve shape in water phantom between (a) electron and (b) photon (Mayles, Nahum & Rosenwald, 2021)

Based on **Figure 2.4**, PDD for an electron beam also differ from photons in term of determination of electron range parameter which is important during the treatment planning. These range concept indicates the distance traveled by an electron beam or the penetration depth of the electron beam. Understanding these factors is essential in order to decide on the appropriate electron energy for the therapy. One of the key parameters to consider during planning is the therapeutic range (R_t) which is the range from the surface to either 80 % or 90 % dose level indicating by R_{80} or R_{90} respectively. This range is critical as it must encompass the distal edge of the target volume, thereby delivering the maximum dose to the tumor volumes (Mott & West, 2021). Besides, the practical range (R_p) is the depth at which the steepest tangent of the electron PDD intersects the bremsstrahlung background line, indicating the depth beyond which no incident electron can penetrate

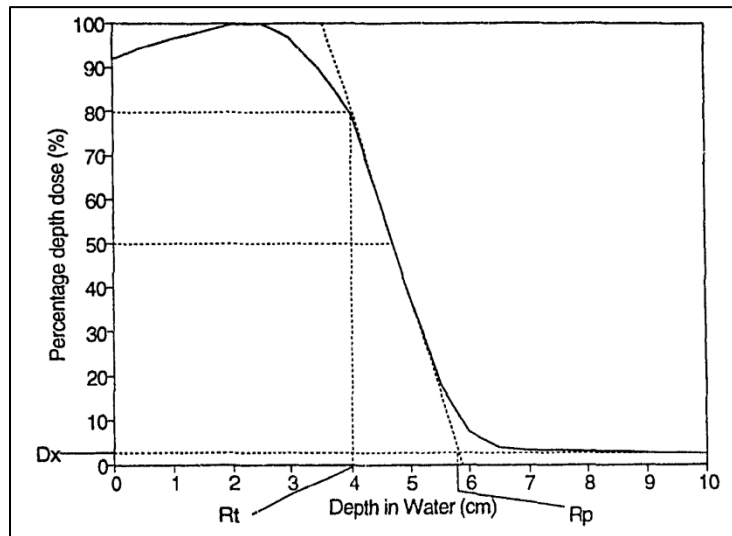


Figure 2.4: Typical electron range parameter used in defining electron PDD curve

Various factors, such as beam energy, field size, and penetration depth can affect the shape of the PDD curve. As the beam energy increases, the electron range increases thus PDD also increases. Lower electron beam energies lead to decreased surface dose levels due to electrons being deflected into larger angles, and also low-energy electron beams exhibit a more rapid dose fall-off. Additionally, PDD has no significant difference when the field size increases. Yet, when the field size is less than the R_p , a noticeable change occurs in the PDD because of the loss of side scatter equilibrium with decreasing field size (Gerbi, Kirova & Orecchia, 2011). On the other, hand, the presence of high density and low-density material also can affect the shape of PDD as shown in **Figure 2.5 (a) and (b)**.

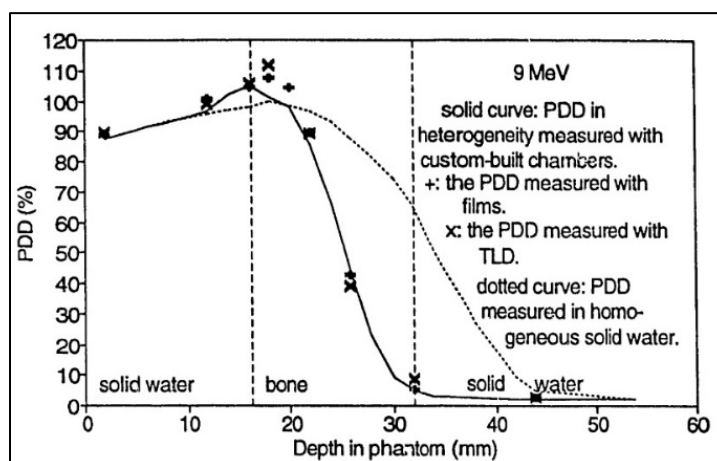


Figure 2.5: Electron PDD curve in inhomogeneous density medium containing bone material (Xiaofang Wang, 1994)

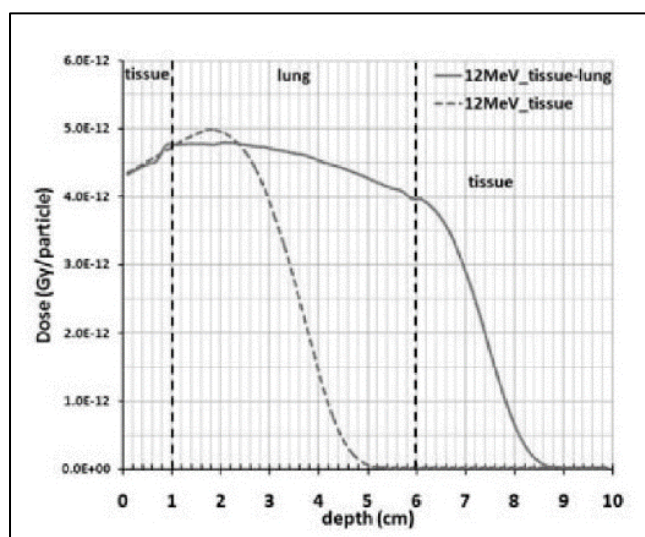


Figure 2.6: Electron PDD curve in inhomogeneous density medium containing lung material (Mihailescu, Borcia & Alexandru, 2018)

When radiation beams pass through phantoms containing dense materials, the doses in front of the inhomogeneity significantly increase due to increased backscattered electrons. However, the overdosing effect will reduce with increasing beam energy (Xiaofang Wang, 1994). Besides, a lower absorbed dose is observed beyond the inhomogeneity due to substantial electron beam attenuation. Furthermore, as the radiation beams pass through phantoms with low-density materials, the dose

values in front of the inhomogeneity usually decrease because backscattering processes decrease, resulting in a higher absorbed dose beyond the inhomogeneity due to reduced energy absorption (Mihailescu, Borcia & Alexandru, 2018).

2.3 Optically Stimulated Luminescence Dosimeter (OSLD)

In recent years, there has been a noticeable rise in the utilization of Al₂O₃:C commercial OSL nanoDot dosimetry, specifically designed for single-point radiation assessment in clinical settings (Musa et al., 2017). The nanoDot OSLD comprises a small chip of Al₂O₃:C, enclosed within plastic disks and water-equivalent light-tight plastic encapsulation. The crystal of Al₂O₃:C contains a trace amount of contaminant that forms crystal lattice imperfection or defect which causes the trapping or recombination of electrons or holes. The crystal's structure comprises the valence band, the conduction band, and the forbidden band (Endo *et al.*, 2012).

OSLD operates on a principle similar to TLD dosimetry, where instead of heat, light is employed to release trapped energy in the form of luminescence. The basic concept of OSLD relies on the detection of blue light emitted irradiated crystalline Al₂O₃:C detector when exposed to green light and the intensity of emitted luminescence is proportional to the absorbed dose. The dosimetric properties of OSLD are primarily governed by two processes which are the trapping of electrons and holes generated by ionizing radiation in defects within the crystal and the optical stimulation of these trapped charges during readout. This stimulation leads to electron-hole recombination and subsequent luminescence (Kry *et al.*, 2020).

Based on **Figure 2.7**, during the irradiation of x-ray, the OSLD will be exposed to ionizing radiation and the energy deposited in the OSLD may give rise to excitation and ionization thus induces the electrons to transition from the valence band to the

conduction band. The lattice defect will trap the electron within the forbidden bands of the crystal structure (Saidin *et al.*, 2021). During the readout process, which occurs inside the reader, a light with a certain wavelength will be exposed to the OSLD thus releases the trapped electron from the defects back to the conduction band. The recombination of electrons and holes will cause the emission of light due to the optical transition of electrons moving between energy bands. Photomultiplier tube (PMT) will then measure the intensity of the blue light emitted in the unit count to determine the absorbed dose (Y. Musa *et al.*, 2017).

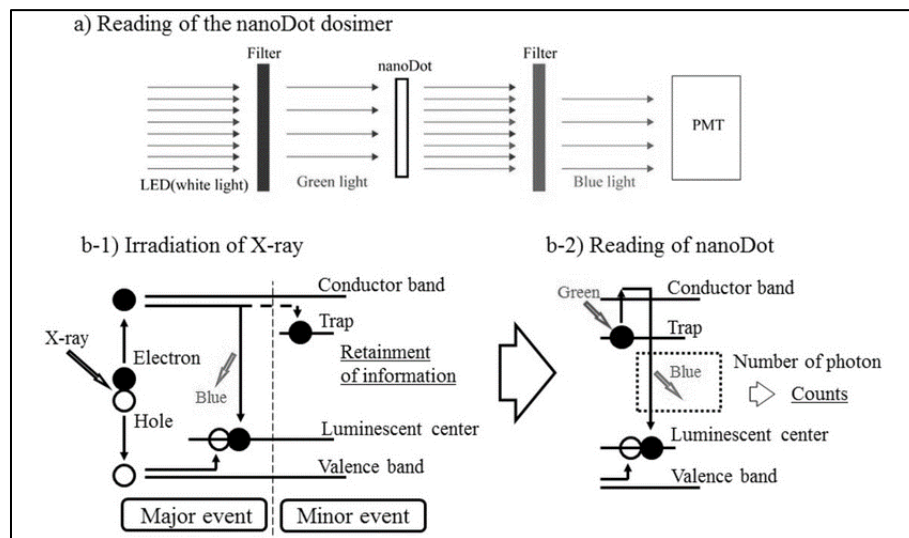


Figure 2.7: Schematic diagram illustrates the fundamental principle of OSLD during (a) reading and (b) irradiation (Takegami *et al.*, 2015)

OSLD shows a high level of sensitivity across the broad spectrum of dose rates and doses utilized in radiotherapy. $\text{Al}_2\text{O}_3:\text{C}$ materials allow for precise control over the intensity and wavelength of stimulation light, facilitating multiple OSL measurements. Furthermore, OSL response typically shows a linear behavior that is not influenced by energy or dose rate, aside from the need to adjust for angular response (Mayles, Nahum & Rosenwald, 2021a). In medical dosimetry, the linear dose-response ranges up to 300

cGy and has a broad energy range from 5 keV to 20 MeV, making it an excellent dosimetry tool (Mohd Yusof et al., 2020). OSLD shows reusability as the radiation signal can be reset by light exposure, although the duration varies based on light intensity and the dose record of the dosimeter.

2.4 Radiochromic Film

Radiochromic film dosimetry is now widely recognized as a dependable passive two-dimensional (2D) method for precise in vivo dosimetry across various applications in radiation physics (Casolaro *et al.*, 2019). The film requires establishing a calibration curve during calibration under known energy conditions. This involves exposing films to a uniform dose distribution at various dose levels. When appropriately calibrated and maintained in suitable environmental conditions, radiochromic film can serve as a relative dosimeter with a better than 3% precision (Resch *et al.*, 2022). Gafchromic EBT films from Ashland ISP, Wayne, NJ, particularly the latest EBT3 film, have gained significant popularity among radiochromic films.

EBT3 film consists of a single active layer approximately 28 μm thick, incorporating the active component, a marker dye, stabilizers, and other necessary elements. This active layer is sandwiched between two 125 μm matte-polyester substrates shown in **Figure 2.8**. The matte surface of EBT3 films has proven advantageous in eliminating Newton rings, which could otherwise affect scanning accuracy (Gungor *et al.*, 2020). Additionally, the symmetrical layer configuration of EBT3 eliminates the orientation dependence on the sides previously observed in EBT2 films (Méndez, Rovira-Escutia & Casar, 2021).

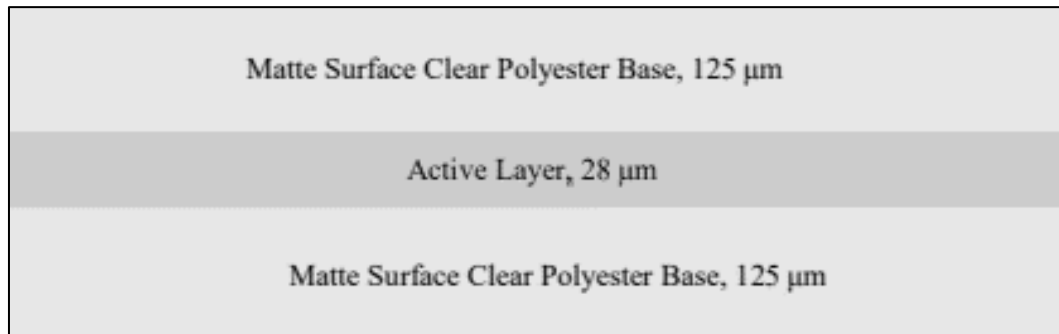


Figure 2.8: Schematic diagram illustrates the composition of EBT3 film (Rohani *et al.*, 2019)

The fundamental principle of film dosimetry involves the alteration of the crystalline structure of its sensitive elements when exposed to ionizing radiation. This process initiates a polymerization within the film's monomers, changing color from colorless to shades of blue upon irradiation (Casolaro *et al.*, 2019). The degree of darkening directly correlates with the level of exposure, with the film becoming darker as the absorbed dose increases due to increase in the optical density as shown in **Figure 2.9**. Scanning the film with a flatbed scanner enables the measurement of changes in the visible absorption spectrum, while specialized software is used to convert scan pixel values into corresponding doses (Méndez, Rovira-Escutia & Casar, 2021).

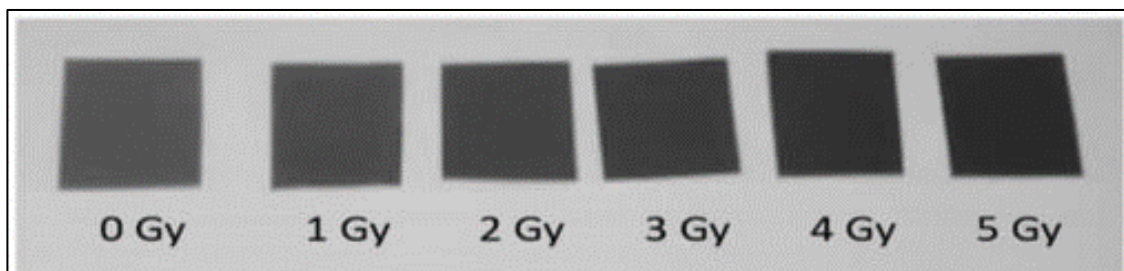


Figure 2.9: Example of film darkening as the dose increases (Musa *et al.*, 2022)

The utilization of EBT3 film in radiotherapy is due to its characteristics resembling tissue or water, along with its excellent spatial resolution and minimal

reliance on energy and dosage (Hariyanto et al., 2023). EBT3 film also provides a convenient and quick method for generating isodose curves or PDD curves for photon, electron, and ion beams (Casolaro *et al.*, 2019). EBT3 film remains reliable and cost-effective for dosimetry measurements in radiotherapy applications, withstanding temperatures up to 60°C and usable for energies up to 25 MeV within a dose range of 0.01 to 10 Gy (Mutsakanyi & du Plessis, 2021).

2.5 Ionization Chamber

The ionization chamber is the most commonly used dosimeter in radiotherapy for quality assurance and accurately measuring machine output. Ionization chambers are available in various designs to suit different applications. The utilization of the parallel-plate ionization chamber is strongly advocated for electron beam dosimetry applications for energy below the 10 MeV threshold. This chamber demonstrates proficiency in measuring electron energies up to 50 MeV (Mihailidis, 2019). A parallel-plate ionization chamber also known as plane-parallel consists of two plane walls made of plastic arranged in parallel as shown in **Figure 2.10**.

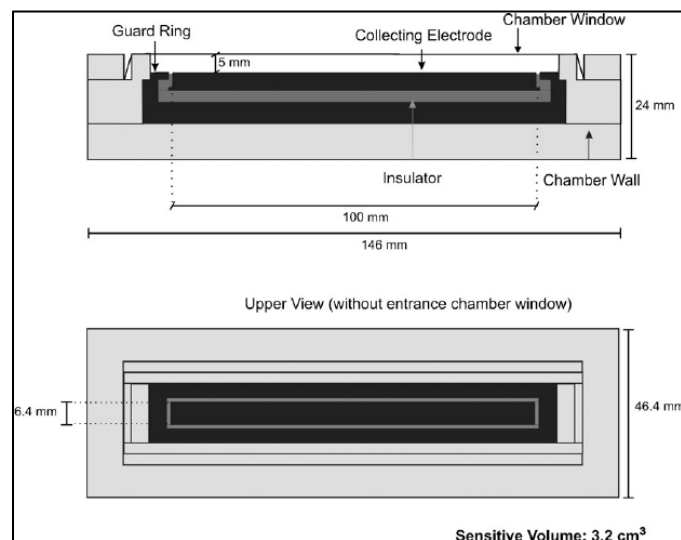


Figure 2.10: Schematic diagram illustrates the component of parallel plate ionization chamber (Maia & Caldas, 2005)

The plane walls are coated with a conducting layer, serving as the positive and negative electrodes. The first wall functions both as an entry window and a polarizing electrode, while the second wall serves as the rear wall, a collecting electrode (anode and cathode), and accommodates the guard-ring system. The region between these walls is filled with gas as collecting volume. The electrodes are positioned close, creating a thin air gap that minimizes noticeable perturbations. Guard electrodes play a critical role in establishing uniform field lines and reducing the settling time of the chamber. Electrometer is employed as readers for ionization chambers (Mayles, Nahum & Rosenwald, 2021).

The fundamental concept of ionization chambers is based on the detection of the charge generated when ionizing radiation interacts with the gas as shown in **Figure 2.11**. This interaction causes high-energy electrons to be released from the chamber wall. Then, some of the electrons penetrate the sensitive volume and ionize air molecules, to form positive (+) ions and low-energy electrons. When the low-energy electrons react with electronegative oxygen molecules, negative (-) ions are formed. The anode and cathode experience an electric potential, creating an electric field that then attracts the positive and negative ions resulting in a current that can be measured by an electrometer (Ross, 2015).

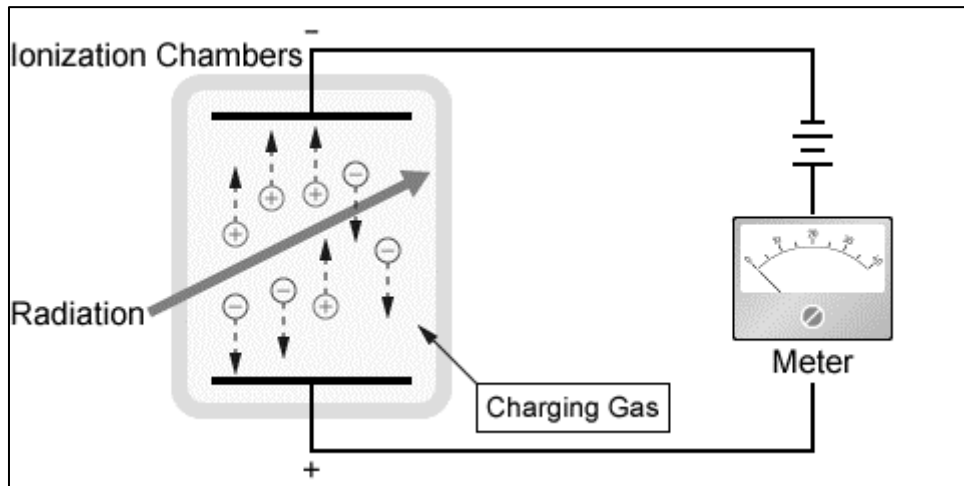


Figure 2.11: Schematic diagram illustrates the fundamental principle of the ionization chamber

Ionization chambers offer numerous advantages over alternative detectors, particularly as they are widely recognized as the standard dosimeter in many dosimetry protocols for precisely measuring the dose. Parallel-plate ion chambers are known for their effective measurement point positioned at the chamber's front plane which offers excellent depth resolution, which makes them ideal for measurements in areas with high dose gradients or where a precise measurement point is essential (Barna *et al.*, 2022). Lastly, it is recommended to use a Cobalt-60 calibrated ionization chamber according to the standard practice for dosimetry protocols and codes of practice. This calibration ensures accurate measurement of absorbed doses in external beam radiotherapy (Solimanian, Ghafoori & Ghafoori, 2010).

2.6 Previous Studies

Xiaofang Wang, (1994) investigated the PDD measurement for 9 to 18 MeV electron beams in a homogeneous solid water phantom, a homogenous bone-like phantom, and a heterogeneous phantom combining solid water and bone-like materials. The study employed custom-built ionization chambers, film, and TLD for

measurements. A comparative analysis was conducted to evaluate the response of film and TLD in measuring PDD with comparison to the ionization chamber. The results indicated that dosimetry based on film and TLD closely corresponded with ionization chamber dosimetry in both homogeneous and heterogeneous phantoms. However, the PDD measured by TLD was slightly higher than film. Additionally, the study highlighted the influence of bone presence within the phantom on the PDD curve.

Mihailescu, Borcia & Alexandru, (2018) investigated PDD measurement for 3 to 19 MeV within inhomogeneous phantoms which include single layers of bone, lung, air, or titanium inserted between soft tissue equivalent material. The measurements were conducted using MC simulations. The study revealed the significant impact of inhomogeneities on electron dose distributions, demonstrating a characteristic "dip and peak" pattern near the inhomogeneity. Specifically, high-density materials led to substantial dose enhancements at the front of the inhomogeneity while low-density materials did not cause notable dose perturbations in surrounding tissues. The presence of lung and air in the phantom had minimal effects on dose distributions compared to high-density materials.

Mohd Yusof et al., (2020) investigated the PDD measurement for a 6 MV photon beam and a 6 MeV electron beam in a homogeneous solid water phantom using OSLD. The obtained PDD was compared to the EBT2 film dosimeter, ionization chamber, and TPS. The measured PDD using OSLD closely aligned with results from the ionization chamber, EBT2 film, and TPS software, displaying discrepancies within 13.4 % and 10.4 % for 6 MV photons and 6 MeV electrons, respectively. The study also revealed that the beam output calibration measured by OSL dosimeters showed good agreement with the ionization chamber, with discrepancies within 1.6 % and 5.9 % for 6 MV

photons and 6 MeV electrons, respectively. Overall, the findings suggested the suitability of OSL for direct dosimetry measurements in both high-energy photons and electrons.

Zabihzadeh et al., (2020) investigated the influence of lung tissue on dose distribution by measuring PDD for a 6 MV photon beam in a water phantom containing lung tissue material with various field sizes measured by an ionization chamber and MC calculations. The study observed that the perturbation of dose in the presence of lung inhomogeneity compared to homogeneous soft tissue was highly dependent on factors such as field sizes, depths, and lung density. In larger field sizes, the absorbed dose in the lung area was greater compared to equivalent depths in inhomogeneous soft tissue. The study also observed that higher lung densities resulted in higher maximum increased doses in lung tissue, and conversely, lower lung densities led to lower maximum increased doses.

Ispir et al., (2021) investigated the accuracy of OSLD in verifying radiotherapy dose calculations in medium with metal implant. PDD measurement was conducted for a 6 MV photon beam in both a homogeneous solid water phantom and an inhomogeneous phantom containing metal implants, using nanoDot OSLDs encased in paraffin materials. The obtained PDD was compared against EBT3 film, pinpoint ion chamber, MC simulations, and the Acuros XB (AXB) algorithm. The study revealed that PDD obtained by OSLD demonstrated strong agreement with measurements from film dosimetry, ionization chamber, MC simulations, and TPS algorithm calculations. In a homogeneous phantom with small field sizes, there were no significant differences in PDD values between OSLDs and other dosimeters. However, the presence of metal

implants caused alterations in the dose distribution near the implants, leading to deviations in PDD values.

Table 2.1: Summary of the previous study with comparison to the present study.

Author	Study	Finding	Comparison with the present study
(Xiaofang Wang, 1994)	Depth Doses and Photon Contamination of Electron Beams in Heterogeneous Phantoms	<ul style="list-style-type: none"> • PDD in a homogeneous phantom measured by film and TLD correspond well with the ionization chamber with a difference of < 3 %. • Significant errors occur in PDD measurement in the inhomogeneous phantom. • PDD measured by TLD is slightly higher than film 	<ul style="list-style-type: none"> • Instead of using TLD, nanoDot OSLD was used and compared to an ion chamber and EBT3 film. • This study only measures PDD at 9 MeV for both bone and lung phantom.
(Mihailescu, Borcia & Alexandru, 2018)	Electron Dose Distributions in Inhomogeneous Phantoms: A Monte Carlo Study	<ul style="list-style-type: none"> • Depth dose distribution accurately calculated with 0.3% statistical error in inhomogeneous tissue phantom by using Monte Carlo simulation. • Dose perturbation is more significant at low energy especially when there's a significant difference in density compared to the surrounding medium. 	<ul style="list-style-type: none"> • This study measure PDD in medium containing bone and lung phantom using dosimeter instead of using MC simulation.
(Mohd Yusof <i>et al.</i> , 2020)	Percentage Depth Dose Measurement in High Energy Photons and Electrons by	<ul style="list-style-type: none"> • The measured PDD by OSLD were in good agreement with the ionization chamber, EBT2 film, and TPS software within a 	<ul style="list-style-type: none"> • This study measure PDD for 9 MeV in the medium consisting of an inhomogeneous

	Using the Al ₂ O ₃ Optically Stimulated Luminescent (OSL) Dosimeter	<ul style="list-style-type: none"> percentage of 10.4% of discrepancies for 6 MeV electrons. OSL signals were in good linearity with the increased dose (MU) for 6 MeV electrons shown by the linear regression (R²) values of close to 1. 	<ul style="list-style-type: none"> density medium instead of a homogenous medium. Instead of using EBT2 film, this study uses EBT3 film
(Zabihzadeh <i>et al.</i> , 2020b)	Effect of lung inhomogeneity on dose distribution during radiotherapy of the patient with lung cancer	<ul style="list-style-type: none"> Maximum increased dose in lung tissue with lung density of 0.5 and 0.25gr/cm³ depending on increased field size. The dose reduction in the lung region was more pronounced for higher photon energies and lower lung density. 	<ul style="list-style-type: none"> This study only using the same lung material with the same density and same beam field size. Instead of a photon beam, this study uses an electron beam.
(Ispir, <i>et al.</i> , 2021)	NanoDot™ OSLDs in verifying radiotherapy dose calculations in the presence of metal implants: Monte Carlo-assisted research	<ul style="list-style-type: none"> The measured dose using OSLDs at deeper depths of the phantom was found to be in good agreement with both EBT3 and IC measurements, as well as MC simulation and AXB algorithm calculations for a medium consisting of aluminium. The implant materials did not significantly affect the data obtained using OSLDs at deeper depths of the phantom. 	<ul style="list-style-type: none"> Bone material was used as a high-density material instead of metal implant. OSLD and EBT3 film were being compared to an ionization chamber instead of TPS and MC Instead of a photon beam, this study uses an electron beam.